Egypt. J. Solids, Vol. (45) (2023)

Structure, properties, and thermal behaviour of chemically synthesized 3-((2,5-Difluorophenyl)diazenyl)-6-ethyl-4-hydrox-2*H*-pyrano[3,2-*c*]quinoline-2,5(6*H*)-dione as new brand organic materials: Antimicrobial activity

H.N. Soliman**, I.S. Yahia

Department of Physics, Faculty of Education, Ain Shams University, P.O. Box 5101, Heliopolis 11771, Roxy, Cairo, Egypt

Receive Date: 26 Jun 2023; Revise Date: 4 Aug 2023; Accept Date: 8 Aug 2023; Publish: 9 Aug 2023

Abstract

Chemical, crystal structures, properties, thermal behaviour, kinetic parameters, and antitumor activity of synthesized 3-((2,5-Difluorophenyl)diazenyl)-6-ethyl-4-hydrox-2*H*-pyrano[3,2-*c*]quinoline-2,5(6*H*)-dione (DFPDAEHPQD) were investigated and characterized. Different techniques are used to identify the structure of DFPDAEHPQD, such as ^{1}H nuclear magnetic resonance (NMR) ^{13}C NMR, X-ray diffraction (XRD) analysis, scanning electron microscopy (SEM), Fourier transform infrared spectroscopy (FTIR), and thermogravimetric analysis (TGA) measurements. XRD analysis showed that DFPDAEHPQD had a polycrystalline nature, and TGA results illustrated that the DFPDAEHPQD was thermally stable up to about 300 ^{o}C. Optical parameters and absorption coefficient of DFPDAEHPQD were calculated using diffused reflectance (DR) measurements in a wide range of wavelengths (200 to 1600 nm). Two optical bandgap values (2.35 and 2.25 eV) were obtained in the applied range of photon energy using Kubelka–Munk theory (KMT). The first value (2.35 eV) is responsible for the direct transition, while the other value (2.25 eV) is responsible for the indirect transition. The AC conductivity obeyed the universal power-law $\sigma_{AC}(\omega) = A\omega^{s}$. Moreover, DFPDAEHPQD showed highly significant antitumor activity and cytotoxicity against two human cancer cell lines: HepG-2 and HCT-116, with the corresponding IC_{50} values of 3.07 and 7.15 µg/ml, respectively. Finally, we hope that DFPDAEHPQD turns out to be environmentally friendly and more energy efficient a novel semiconductor for safe use in various electronic and biomedical applications.

Keywords:

DFPDAEHPQD; organic semiconductors; UV/V is spectroscopy optical properties; anticancer molecules; cytotoxicity and antitumor activity.

*Corresponding author: *E-mail address*:hany.nazmy853@gmail.com (H.N. Soliman).

1. Introduction

Commercialization of organic semiconductors includes display applications, lighting applications, and photocopier machines [1-3]. Furthermore, there is a good suggestion for some new brand organic materials to be examined. One of the advantages of organic electronics is the nearly unlimited choice of materials. Therefore, large industrial applications are involved nowadays and in the future exploitation of organic semiconductors.

Quinolones and their derivatives can work as natural antimicrobials, signaling molecules, and anticancer drugs [4-6]. Fluoroquinolones are the majority of quinolones in clinical use. This is because the physical and structural properties of the quinolones were affected greatly by changing the electronic nature of the replacing atoms or groups [7-12].

The fluorine atom has the highest electronegativity of any element and has a small covalent radius [13]. This causes fluorine's high reactivity and strong bonds to other atoms. Behind the Si–F single bond, C–F bond is the 2nd strongest single bond in organic chemistry [14] and stabilizes organofluorines [15].

Several fluorine compounds are used in electronics [16]. About thirty percent of agrichemicals contain fluorine [17]. Recent studies show that topical fluoride reduces dental caries (Tooth decay) [18]. One of the fluorinated compounds, the cholesterol-reducer atorvastatin (Lipitor), made more income than any other drug until it became common in 2011 [19]. Furthermore, many drugs are fluorinated to retard inactivation and extend dosage intervals because of the stability of the C–F bond [20].

Recently, fluoroquinolones are among the most valuable antimicrobial materials used in human and animal medicine because of their physicochemical and spectrum properties. They have a relatively simple molecular nucleus, which is amenable to many structural modifications. They play major roles in curing dangerous bacterial contagions, essentially infections acquired from hospitals and others [21-25]. Several recent studies have confirmed that fluoroquinolones cause children little or no additional risk compared with other antibiotics [26,27]. Besides the antibacterial activity of fluoroquinolones, recent studies have shown that they are used as anticancer agents because they prevent the enzyme mammalian topoisomerase II [28-33].

Egypt. J. Solids, Vol. (45) (2023)

Pyran is a non-aromatic ring containing 5 carbon atoms, 1 oxygen atom, and 2 double bonds, and its molecular formula is C_5H_6O. Many pyran derivatives are important biological compounds and display antimicrobial, antitumor, and anticonvulsant [34,35]. Azo compounds have broad pharmaceutical, cosmetic, food, and other applications because of their distinctive physicochemical properties and biological activities [36-38]. Moreover, they cause danger to health and the environment because of cancer and mutations.

Based on the topics mentioned above, the main purpose of the work presented here has been to synthesize and develop environmentally friendly and more energy efficient DFPDAEHPQD, which contain quinolone, pyran, azo, and difluoro aryl in one molecular structure as a promising novel anticancer agent as well as a new brand semiconductor for safe use in various electronic and biomedical applications.

2. Experimental Details

2.1. Synthesis of DFPDAEHPQD

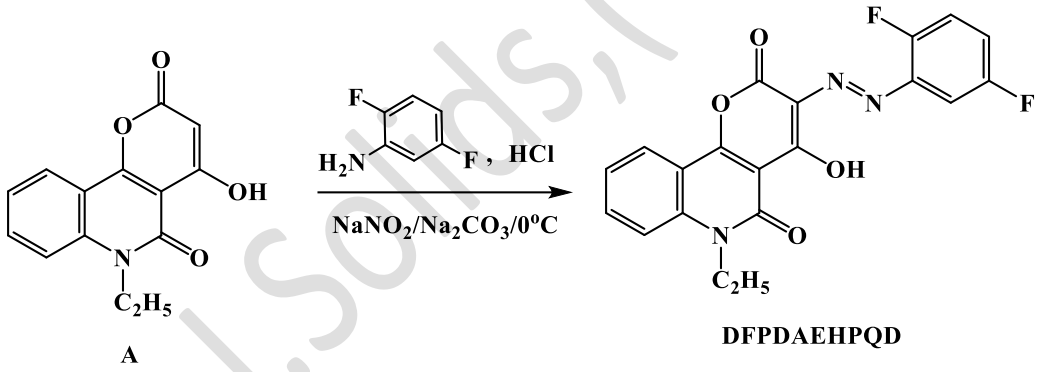

Scheme 1

The reaction mixtures' thin-layer chromatography (TLC) analysis was achieved on Fluka analytical silica gel 60 F254 nm TLC plates. Melting points were measured using Sanyo Gallenkamp MPD 350-BM 3.5. Infrared spectra were recorded on Thermo Nicolet Nexus 470 FT-IR spectrophotometer (cm^{-1}). Varian 400 MHz spectrometer was used to measure ^{1}H NMR (400 MHz) and ^{13}C NMR (100 MHz) spectra. Elemental analyses were done with the aid of the usage of A EuroEA 3000 Elemental Analyzer (Italy). The mass spectrum was achieved on Finnigan 2000, Thermo Quest GC/MS. A triple-quadruple tandem mass spectrometer was attached with electrospray ionization. Compound **A** was prepared according to the reported literature method [39]. To a previously cooled solution (0-5 °C) of compound **A** (1.4 g, 5 mmol) in sodium carbonate solution (Na_2CO_3, 50 ml,

1M), a solution of freshly prepared diazonium chloride from 2,5 difluoroaniline, (0.5 ml, d =1.28 g/ml, 5 mmol) and HCl acid (60 ml, 1M), was added with stirring continuously. After completion of the addition, the reaction mixture was stirred at 25 °C for 2 h. The formed precipitate was filtered off, washed with water, dried, and recrystallized from AcOH to give DFPDAEHPQD compound (1.27 g, 65%), m.p = 270-272 °C yellow DFPDAEHPQD (Scheme 1). M.F: $C_{20}H_{13}F_2N_3O_4$, **IR (KBr, cm^{-1}):** 3421 broadband (OH), 3087 ($CH_{aromatic}$), 2991, 2942 ($CH_{aliphatic}$), 1745 ($C=O_{\alpha\text{-}pyrone}$), and 1676 ($C=O_{quinoline}$), 1616 (C=C), 1573 ($N=N_{azo}$.). ^{1}H NMR (400 MHz, DMSO-d_6) d ppm: 1.37 (t, J=8.00 Hz, 3H, CH_3), 4.38 (t, J=8.00 Hz, 2H, N-CH_2), 6.93 - 7.02 (m, 1H$_{phenyl}$), 7.13 - 7.22 (m, 1H$_{phenyl}$), 7.35 (t, J=8.00 Hz, 1H, C9-H), 7.42 (d, J=8.00 Hz, 1H, C7-H), 7.73 - 7.82 (m, 2H, (1H$_{phenyl}$ + 1H, C8-H), 8.33 (dd, J=8.00, 1.57 Hz, 1H, C10-H), 13.24 (s, 1H, C4-OH). ^{13}C NMR (101 MHz, DMSO-d6) δ ppm 13.05 (s, 1C2`), 37.72 (s, 1C1`), 90.23 (s, 1C3), 99.94 (s, 1C4a), 107.60 (s, 1C10a), 113.73 (s, 1C$_{phenyl}$), 115.49 (s, 1C$_{phenyl}$), 116.52 (s, 1C7), 123.05 (s, 1C$_{phenyl}$), 124.31 (s, 1C10), 124.61 (s, 1C9), 125.25 (s, 1C$_{phenyl}$), 134.86 (s, 1C8), 138.09 (s, 1C6a), 149.1 (s, 1C10b), 151.55 (s, 1C$_{phenyl\ F}$), 159.36 (s, 1C$_{phenyl\ F}$), 160.97 (s, 1C2), 162.64 (s, 1C4), 169.14 (s, 1C5) [40,41].

2.2. Devices and measurements

A pellet with dimensions, 13 mm diameter and 1 mm thick was obtained using the manual hydraulic press. The description of the used method was mentioned earlier [42]. The surface morphology of the DFPDAEHPQD in powder form was obtained using SEM type (JSM-6360) operated at 20 kV. XRD measurement of the DFPDAEHPQD sample was achieved with a Shimadzu LabX-XRD-6000 X-ray diffractometer at ambient temperature using filtered CuK_α radiation (λ = 1.5406Å). XRD pattern was recorded automatically over a wide range of diffraction angles (5–80°). Thermal analysis of DFPDAEHPQD has been achieved by thermo-gravimetric analysis (TGA-50) in a nitrogen atmosphere up to 700°C temperature. The UV/visible spectra of DFPDAEHPQD were recorded using an integrating sphere system connected to a UV-3600 spectrophotometer (Shimadzu, Japan) inside a wavelength range of 200 – 1600 nm. FTIR spectrum of DFPDAEHPQD was measured on THERMO SCIENTIFIC, DXR FT-IR Spectrometer through the region between 4000 and 400 cm^{-1} wavenumber. About 2% of finely crushed DFPDAEHPQD powder was mixed with potassium bromide to get 100 mg of the subjected sample to this analysis. The electrical characterization measurements of DFPDAEHPQD films were achieved at a constant

temperature (25 °C) using properly computer-controlled Keithley 4200-SCS over an extensive variety of frequencies beginning from 3 kHz up to 10 MHz.

2.3. Cytotoxic of DFPDAEHPQD

The cytotoxic examination was achieved at the Regional Center for Mycology and Biotechnology, Al-Azhar University. The used two human cancer cell lines, namely: HepG-2 (hepatocellular carcinoma) and HCT-116 (colon carcinoma) were purchased from VACSERA, Unit of Tissue Culture, Cairo, Egypt. The inhibition zone was measured at each well after 24 h at 37 °C.

For cytotoxicity assay, 1×10^4 cells (HepG-2 and HCT-116) per well in 100 µl of growth medium were seeded in a 96-well plate. The used procedure was mentioned earlier in advance [43]. After treatment with the characteristic compound, the survival curve for each tumor cell line was obtained by plotting the relation between surviving cells against drug concentration. The concentration necessary to induce toxic effects in 50% (IC_{50}), of intact cells, was determined by plotting the relationship between percentages of cell viability against sample concentration using GraphPad Prism software (San Diego, CA, USA) [44].

3. Results and Discussion

3.1. Fourier transformation infrared spectroscopy (FTIR) of DFPDAEHPQD

FTIR became a vital instrument in various fields and is considered a fingerprinted analysis. FTIR spectrum of DFPDAEHPQD within 400–4000 cm^{-1} of wavenumber range is presented in Fig. 1. As presented in Fig. 1, there are two strong absorption peaks at 3441.32 cm^{-1} of a broadband (OH) and 3080.99 cm^{-1} of ($CH_{aromatic}$). Moreover, three peaks were observed at 2978.51, 2932.23, and 2353.72 cm^{-1} that refer to ($CH_{aliphatic}$), 1755.37 cm^{-1} of ($C=O_{\alpha\text{-}pyrone}$), 1672.73 cm^{-1} of ($C=O_{Quinoline}$), 1609.92 cm^{-1} of (C=C) and the peaks within the range 1563.64-1414.88 cm^{-1} are due to azo group N=N [40,41]. An extra two peaks at 1289.26 and 1123.97 cm^{-1} were located due to strong C-F bonds [45].

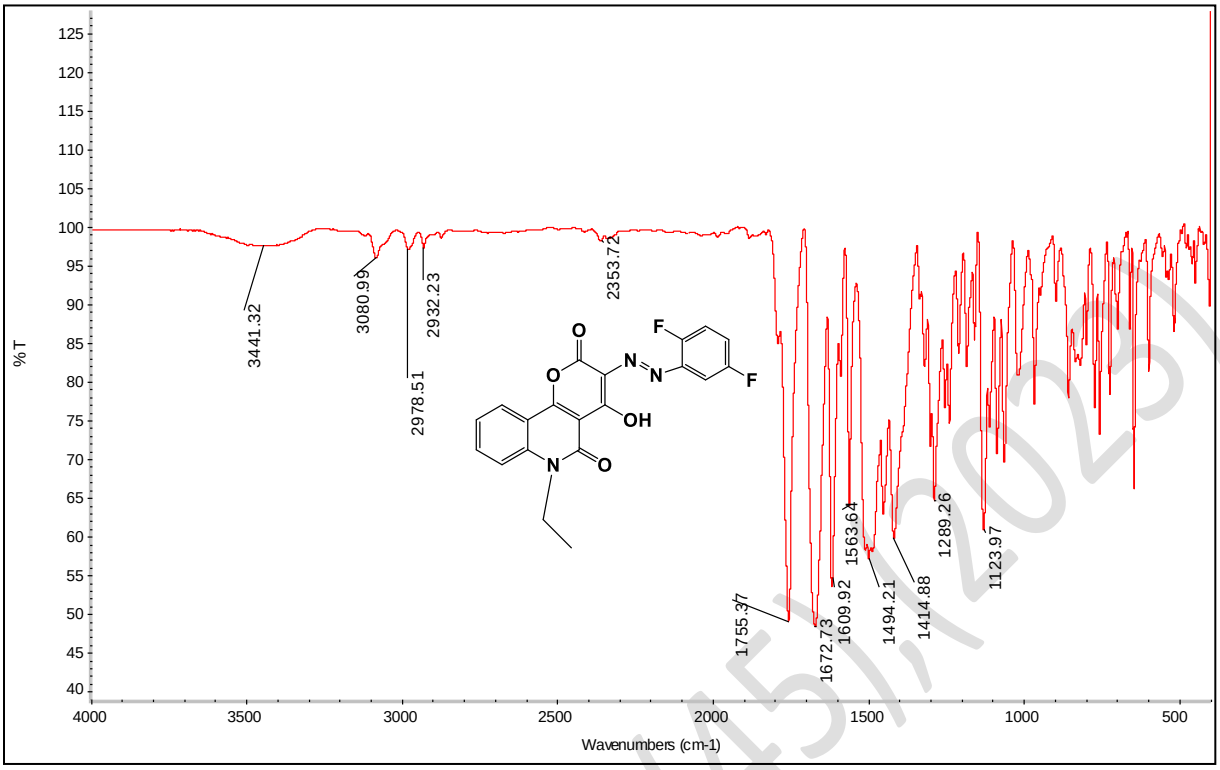

Figure 1. FTIR spectra of DFPDAEHPQD.

3.2. ^{1}H-NMR, ^{13}C-NMR, and mass spectra of DFPDAEHPQD.

Figure 2 shows ^{1}H NMR spectrum of DFPDAEHPQD that revealed the disappearance of aromatic proton at position 3 of *N*-ethylpyranoquinolinone and confirmed the appearance of new three protons in the aromatic region corresponding to the phenyl ring of 2,5-difluoroaniline. ^{13}C NMR spectrum of DFPDAEHPQD exhibited two signals in the aliphatic region attributed to two carbons of the *N*-ethyl group and eighteen sp^2-hybridized carbons in the region δ 90-169 ppm corresponding to the aromatic carbon atoms which are compatible with the number of carbon atoms in the molecular formula of the DFPDAEHPQD as shown in Fig. 3.

Egypt. J. Solids, Vol. (45) (2023)

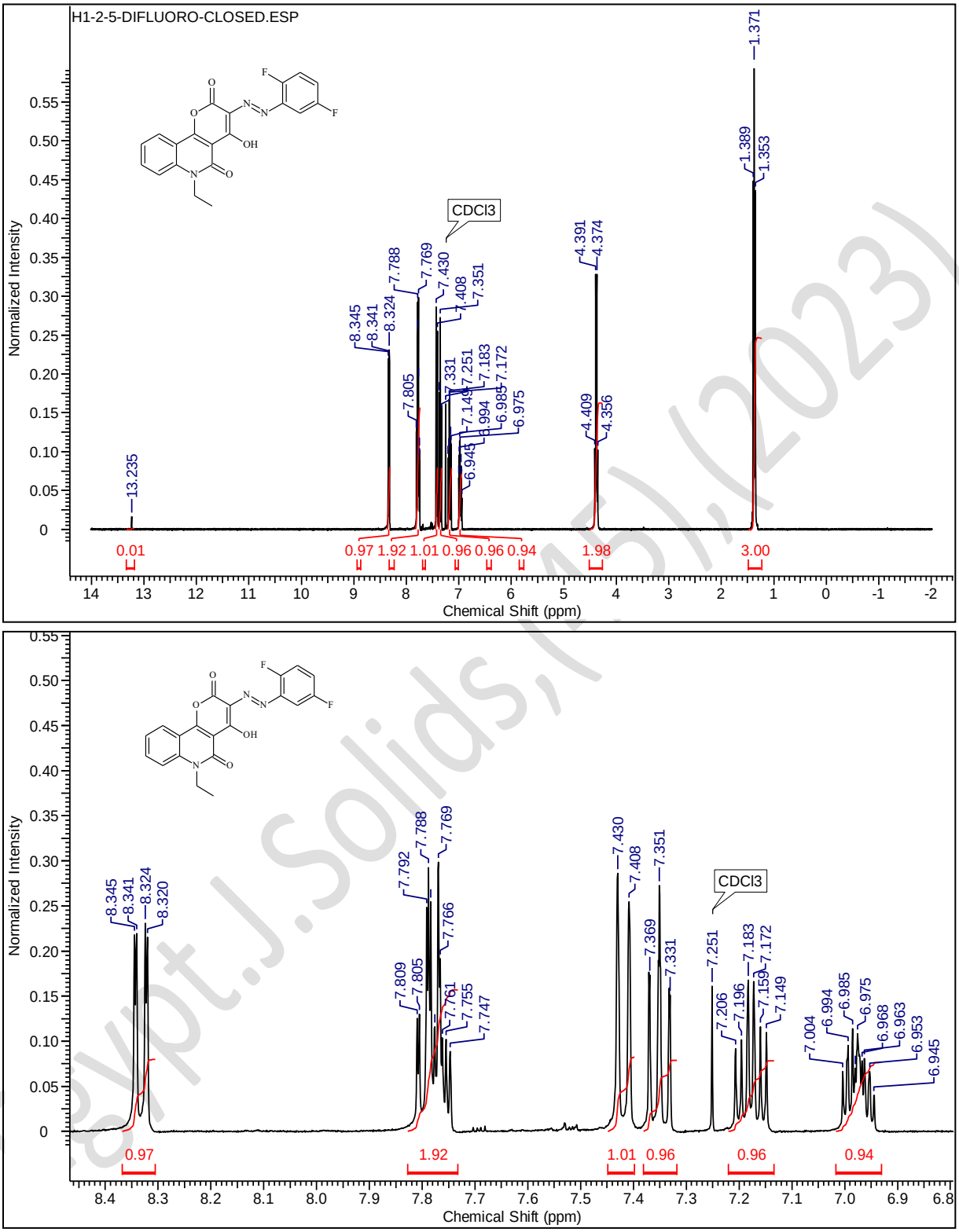

Figure 2. ^{1}H-NMR spectrum of DFPDAEHPQD.

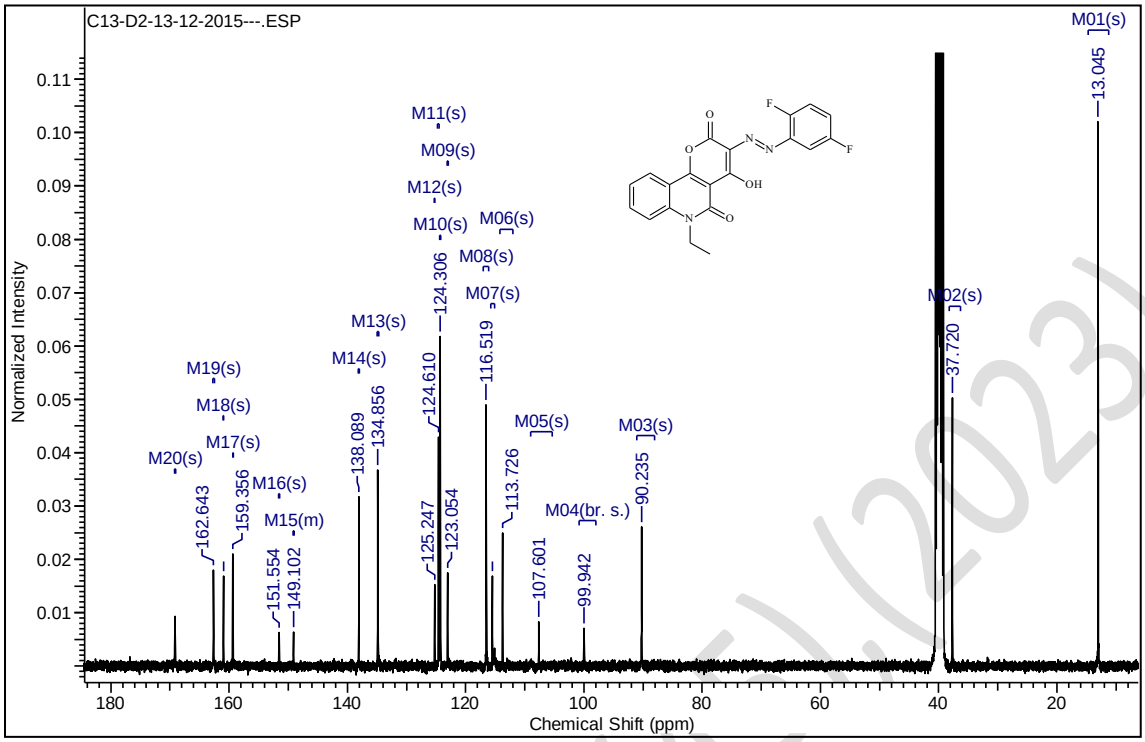

Figure 3. ^{13}C-NMR spectrum of DFPDAEHPQD.

3.3. Surface morphology of DFPDAEHPQD

The SEM micrograph shown in Fig. 4, illustrates the surface morphology of DFPDAEHPQD. This figure shows the formation of a rod-like structure with an average diameter of 0.565 µm. Furthermore, nanorods with various sizes and shapes were randomly distributed. These nanoscale structures are characterized by high sensitivity and may be advantageous in the applications of different fields [46-50].

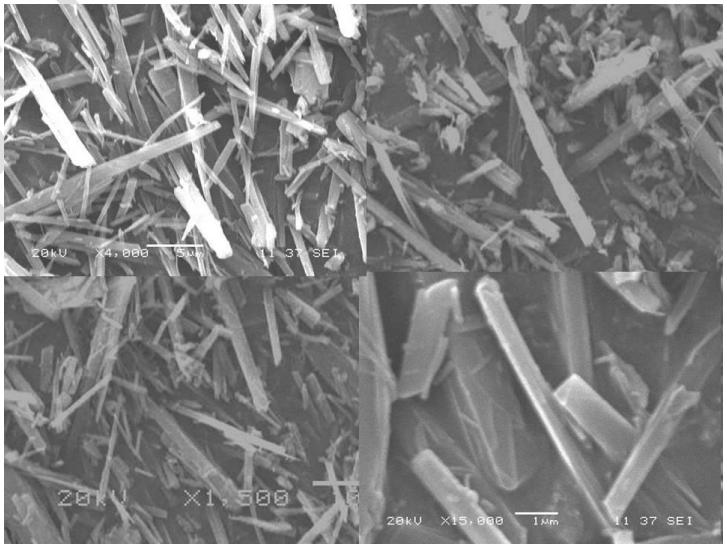

Figure 4. SEM images of different scales of DFPDAEHPQD.

Egypt. J. Solids, Vol. (45) (2023)

3.4. Crystal structure of DFPDAEHPQD

X-ray crystallographic and structural data of DFPDAEHPQD powder are summarized in Tables 1(a&b) with *(hkl)* planes using crysfire and check-cell software [51], and the XRD pattern of the synthesized DFPDAEHPQD is shown in Fig. 5. According to the XRD pattern presented in Fig. 5, it can be concluded that DFPDAEHPQD has a crystalline nature. Analysis of the obtained data in Tables 1(a&b) explained that DFPDAEHPQD is a monoclinic structure with a space group P_2.

Table 1a. XRD analysis of DFPDAEHPQD.

h	*k*	*l*	2Theta, (observed)	2Theta, (Calculated)	Difference
-1	***0***	***1***	6.0148	6.0414	-0.0266
1	***0***	***1***	9.6466	9.6375	0.0091
-2	***0***	***0***	10.97	10.9307	0.0393
0	***0***	***2***	11.8316	11.8166	0.015
0	***1***	***0***	12.435	12.4465	-0.0115
-1	***1***	***1***	13.89	13.8457	0.0443
1	***0***	***2***	15.11	15.047	0.063
-1	***1***	***2***	16.405	16.3969	0.0081
0	***0***	***3***	17.735	17.7646	-0.0296
-3	***1***	***0***	20.6616	20.6623	-0.0007
-3	***1***	***3***	22.123	22.1025	0.0205
0	***0***	***4***	23.8	23.7612	0.0388
-4	***1***	***3***	24.822	24.824	-0.002
-1	***2***	***1***	25.7923	25.7845	0.0078
1	***0***	***4***	26.6434	26.6736	-0.0302
-2	***2***	***2***	27.9	27.8989	0.0011
-5	***1***	***3***	28.42	28.4035	0.0165
2	***2***	***1***	29.045	29.0743	-0.0293
0	***2***	***3***	30.87	30.8728	-0.0028
3	***1***	***3***	31.85	31.8451	0.0049
5	***1***	***1***	33.23	33.2371	-0.0071
5	***0***	***2***	34.65	34.6521	-0.0021
-6	***0***	***6***	36.88	36.8644	0.0156
0	***1***	***6***	38.2	38.208	-0.008
-5	***1***	***7***	41.095	41.1234	-0.0284
-8	***1***	***1***	44.344	44.3441	-0.0001
-12	***0***	***2***	64.625	64.6349	-0.0099

Table 1b. XRD parameters of DFPDAEHPQD.

Lattice parameters						
a	***b***	***c***	***alpha***	***beta***	***gamma***	***volume***
17.9788	7.1059	16.6351	90	115.88	90	1912.047

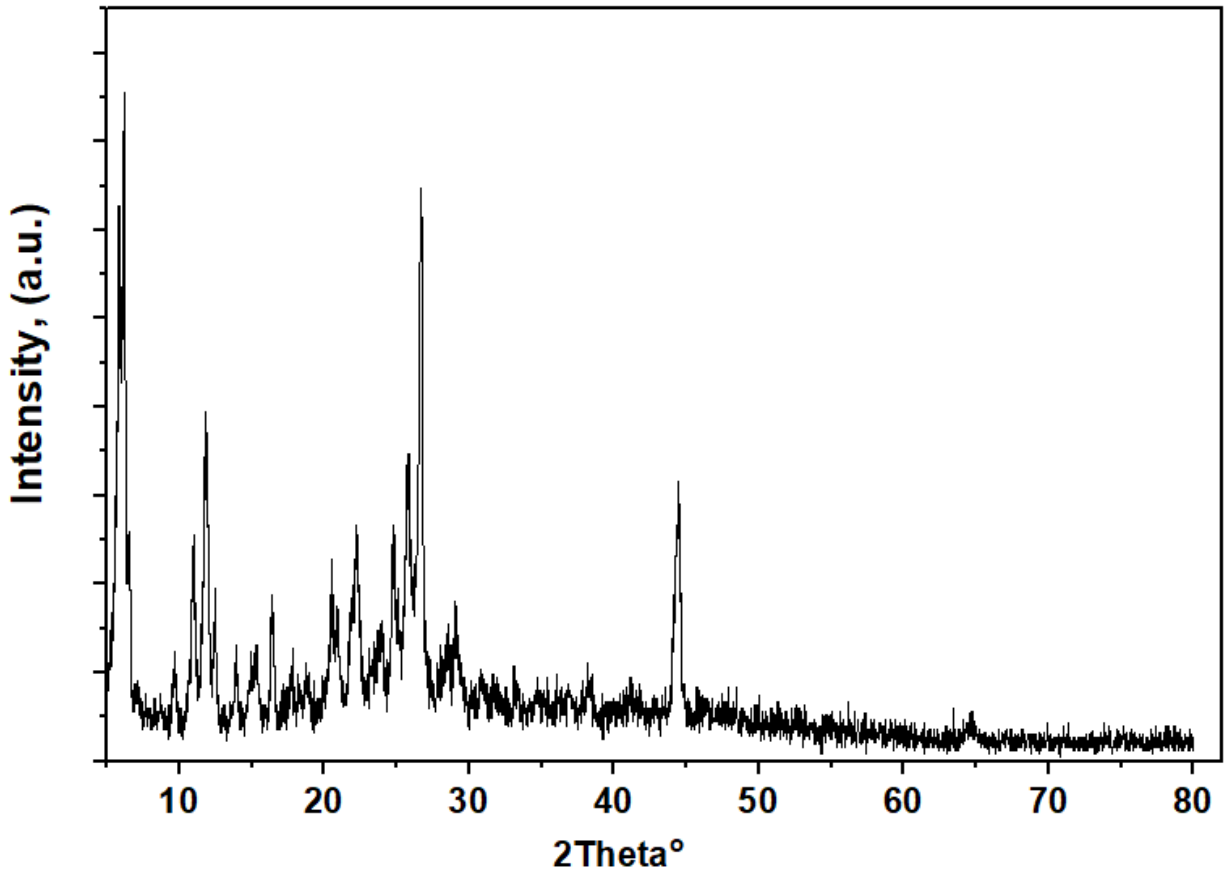

Figure 5. XRD pattern of DFPDAEHPQD.

3.5. Thermal analysis of DFPDAEHPQD

The studied sample's thermogravimetric analysis (TGA) has been achieved and illustrated in Fig. 6. This figure showed that a process of single-stage decomposition was observed in the temperature range (25 – 300 °C). However, beyond this temperature range, the decomposition of the sample caused a significant weight loss at a temperature range of 300 – 400 °C. Moreover, a further increase in decomposition temperature up to 700 °C caused a slow rate of weight loss in the test sample. These analyses confirm that DFPDAEHPQD is a thermally stable organic semiconductor via various temperatures. The high thermal stability in the case of the DFPDAEHPQD up to about 300 °C might be due to the formation of a C–F strong bond [13].

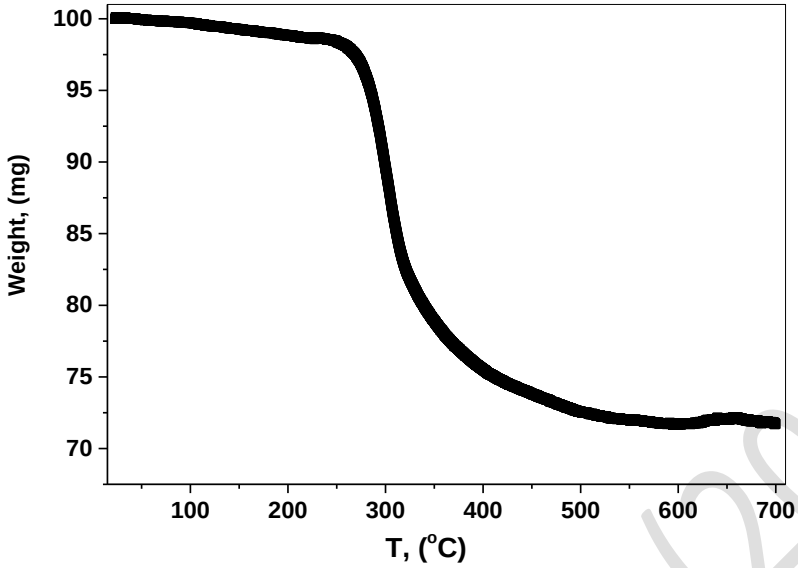

Figure 6. TGA curve of DFPDAEHPQD at a heating rate of 10 ^{o}C.min^{-1}.

3.6. Optical diffused reflectance and absorption index of DFPDAEHPQD.

Measurement of optically diffused reflectance with a UV-visible spectrophotometer is considered as a standard technique for obtaining information about the absorption properties of the material under investigation. Optical diffused reflectance (ODR) and absorption index of the DFPDAEHPQD versus wavelength in the range 200 – 1600 nm, as shown in Figs. 7(a&b). It's obvious from Fig. 7a that the ODR of DFPDAEHPQD didn't change in the 200 – 500 nm range. Then, a sharp increase of the ODR was observed within various wavelengths from 500 to 700 nm, forming the bandgap. After that, the ODR depicted absorption peaks (maximal/minimal peaks) within 700 – 1600 nm of the wavelength range. Light absorbed by the studied material creates these absorption bands [52,53].

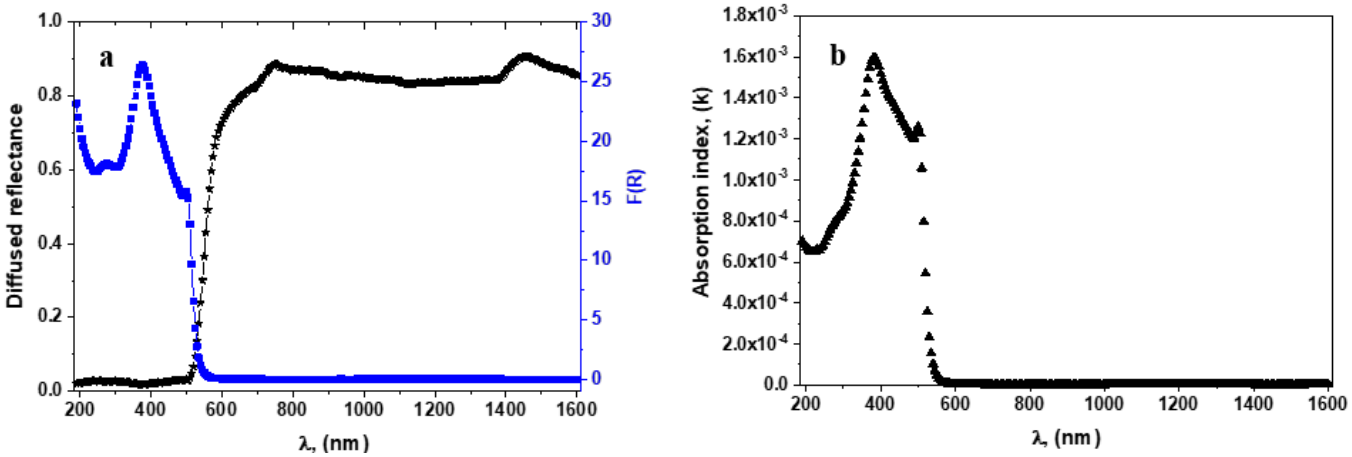

Figures 7(a&b). Diffused reflectance and absorption index of DFPDAEHPQD.

Figure 7b shows that DFPDAEHPQD has small absorption index values ($10^{-4} - 10^{-3}$) due to the non-absorbing area of the DFPDAEHPQD surface, and the inclination of the DFPDAEHPQD sample to the incident light. Also, this figure represents maximum absorption at a wavelength of about 380 nm, typical for band-to-band electronic transitions ($\pi \rightarrow \pi^*$) [54,55]. This sharp peak and the exciton absorption indicate that the DFPDAEHPQD has a very good optical quality, i.e., contains a small density of defects. The optical bandgaps E_g of the DFPDAEHPQD were calculated using Tauc's model as given below [56-58]:

$$F(R) = \frac{(1-R)^2}{2R}, \quad \textbf{(1)}$$

$$\alpha = \frac{F(R)}{t}, \quad \textbf{(2)}$$

$$\alpha h\nu = A(h\nu - E_g)^n, \quad \textbf{(3)}$$

Where *F(R)* is the reflectance which represents the Schuster-Kubelka-Munk model, *R* is the ODR of the layer measured immediately from the spectrophotometer and expressed as a decimal fraction, α is the absorption coefficient, *t* is the sample's thickness (= 0.5 mm), $h\upsilon$ is the energy of the incoming photon, *A* is the band tailing parameter [59] and E_g is the bandgap energy of the sample. In the above equation, *n* = ½ for direct allowed transition, *and* $n = 2$ for indirect allowed transition. Hence, the equation for direct bandgap material is:

$$(\alpha h\nu)^2 = A^2(h\nu - E_g), \quad \textbf{(4)}$$

And the equation for indirect bandgap material is:

$$(\alpha h\nu)^{1/2} = A^{1/2}(h\nu - E_g), \quad \textbf{(5)}$$

Figure 8 shows the plots of $(\alpha h\upsilon)^{1/2}$, and $(\alpha h\upsilon)^2$ versus $(h\upsilon)$ for DFPDAEHPQD in powder form. The bandgaps were obtained via the line interception of these plots to the x-axis at which $\alpha^{1/2}$ and α^2 equal zero. Two optical band gaps (2.35 eV & 2.25 eV) of DFPDAEHPQD were obtained in the studied range of photon energy. The first value (2.35 eV) is responsible for the direct allowed transition, while the other value (2.25 eV) is responsible for the indirect bandgap. These values were found to be higher than those obtained for Pyronin Y [60] and lower than those acquired for DPQ, DPQ-Cl, and DPQ-Cl_2 [61].

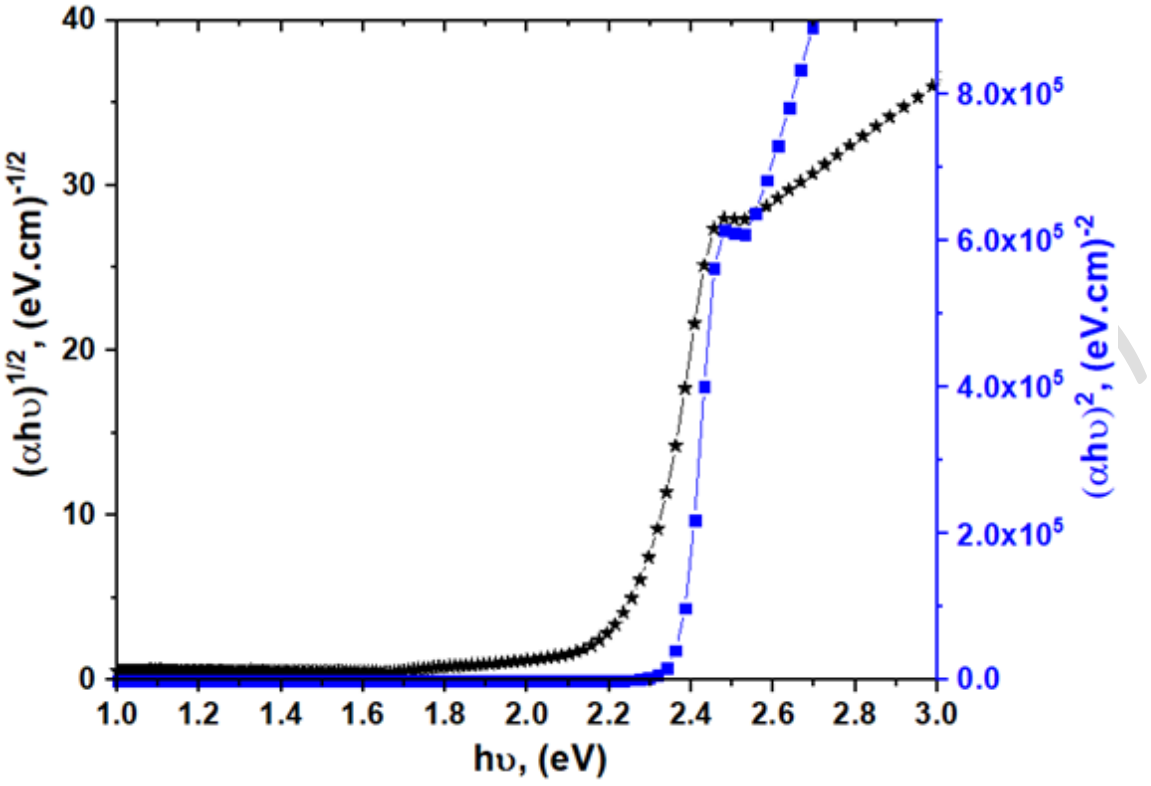

Figure 8. Plot of $(\alpha h\upsilon)^{1/2}$ and $(\alpha h\upsilon)^2$ vs. $h\upsilon$ for DFPDAEHPQD.

3.7. Dielectric behavior and AC electrical conductivity of DFPDAEHPQD

The dielectric function describes the direct response of the material to electromagnetic radiation, and it predominates the behaviour of electromagnetic wave propagation in the material. Therefore, it's essential to recognize the nature of the dielectric function and its basis. The following equations were used to represent the complex dielectric function $\varepsilon^*(\omega)$ for the considered organic material [62]:

$$\varepsilon^*(\omega) = \varepsilon_1(\omega) + i\varepsilon_2(\omega), \quad \textbf{(6)}$$

where

$$\varepsilon_1 = n^2 - k^2, \ \varepsilon_2 = 2nk \quad \textbf{(7)}$$

where $\varepsilon_1(\omega)$ and $\varepsilon_2(\omega)$ are real and imaginary parts of the dielectric constant, respectively. n and k are real and imaginary components of the refractive index, respectively. While the fundamental component $\varepsilon_1(\omega)$ of the dielectric constant describes the refraction of light, the imaginary component $\varepsilon_2(\omega)$ is related to its extinction, and it mainly describes the electron transition from occupied states to unoccupied ones. Plots of $\varepsilon_1(\omega)$ and $\varepsilon_2(\omega)$ versus the applied frequencies for DFPDAEHPQD are illustrated in Fig. 9.

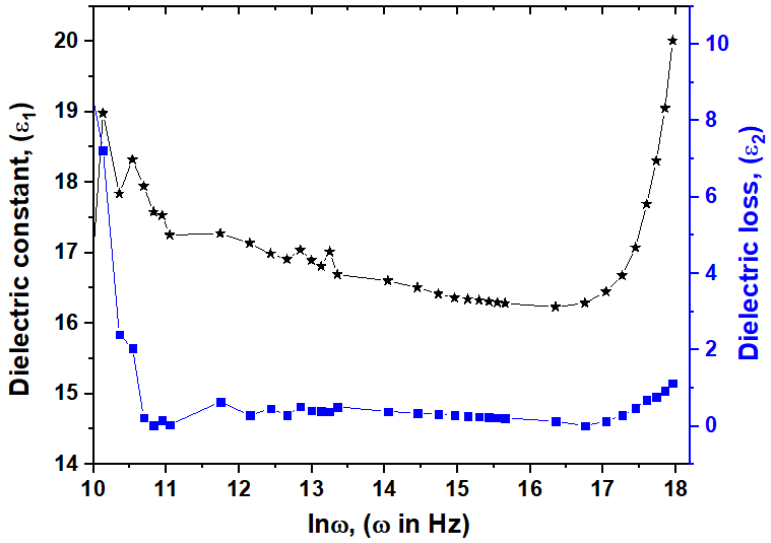

Figure 9. Plots of dielectric constant and dielectric loss versus the applied frequencies for DFPDAEHPQD.

In low-frequency areas, the dielectric constants significantly decrease with the increase in frequency up to 6×10^4 Hz; then, they slightly decrease with the increase of photon frequency. The enhancement of dielectric constants with decreased frequency reveals that DFPDAEHPQD exhibits strong interfacial polarization at a lower frequency. At higher values of photon frequency, the dielectric constant increases and reaches a maximum value when the frequency reaches about 6×10^7 Hz. Furthermore, the amounts of dielectric loss decrease to the smallest possible value and once more increase. Generally, the diminishing dielectric constants of the studied material are related to the mechanism of dielectric polarization. Whereas applying an external electric field to DFPDAEHPQD, exclusive kinds of dielectric polarization can come about as electronic, ionic, dipolar, or interfacial polarization. Electronic and ionic polarizations are the predominant polarization in the high-frequency range. The large value of $\varepsilon_1(\omega)$ at a totally low-frequency range may be interpreted by way of interfacial polarization that occurs by charge carriers, that immigrate and are restricted by defects and gathered while the material is a dielectric. The value of $\varepsilon_1(\omega)$ begins to grow at a high-frequency range because the dipole oscillation can rotate rapidly [63]. The influence of frequency on AC electrical conductivity has been examined to describe the conduction behaviour of DFPDAEHPQD. The following subsequent equations have been used to calculate the AC conductivity of the sample [64-67]:

$$\sigma_{Total.AC}(\omega)=\frac{t}{ZA}, \quad \textbf{(8)}$$

$$\sigma_{Total.AC}(\omega)=\sigma_{DC}(\omega\to0)+\sigma_{AC}(\omega), \quad \textbf{(9)}$$

$$\sigma_{AC}(\omega) = A\omega^{S}, \quad \textbf{(10)}$$

Where $\sigma_{Total.AC}(\omega)$ is the total AC electrical conductivity, Z is the impedance, A is a temperature-dependent constant, $\sigma_{DC}(\omega \to 0)$ is the DC electrical conductivity, $\sigma_{AC}(\omega)$ is the AC electrical conductivity, ω is the angular frequency and s is a parameter (called frequency exponent) which determines AC conduction. Organic semiconductors denote semiconducting organic compounds exhibiting electronic conductivities between 10×10^{-9} and 10×10^{3} $\Omega^{-1}.cm^{-1}$ [68]. The frequency exponent s is a specific parameter showing the numerous-material interactions of charge carriers and impurities. The value of this exponent depends on both frequency and temperature and changes from 0 to 1; it is identical to 1 for typical Debye-type materials.

Moreover, this exponent is related to the charge carriers or extraneous dipoles caused by the existence of impurities and imperfections. In particular, the value of this exponent generally varies from 0.6 to 0.8 in conducting disordered materials, while it is close to 1 in highly disordered dielectrics [69]. Based on the power mentioned above in the law (Eq. 10), the quantity $ln\sigma_{AC}(\omega)$ was plotted against $ln(\omega)$ which is illustrated in Fig. 10. Figure 10 shows that $ln\sigma_{AC}(\omega)$ rises with increasing $ln(\omega)$. The value of the exponent s for DFPDAEHPQD at room temperature was computed by using the slope of the linear part of this relation. In this work, the obtained value of s was 1.0152 ± 0.00318 [60]. This behaviour can be explained in terms of the correlated barrier hopping between centers forming intimate valence alternation pairs [70]. A common feature in arranged, disarranged, organic and inorganic materials is the direct changes of the AC electrical conductivity with the applied frequency [68].

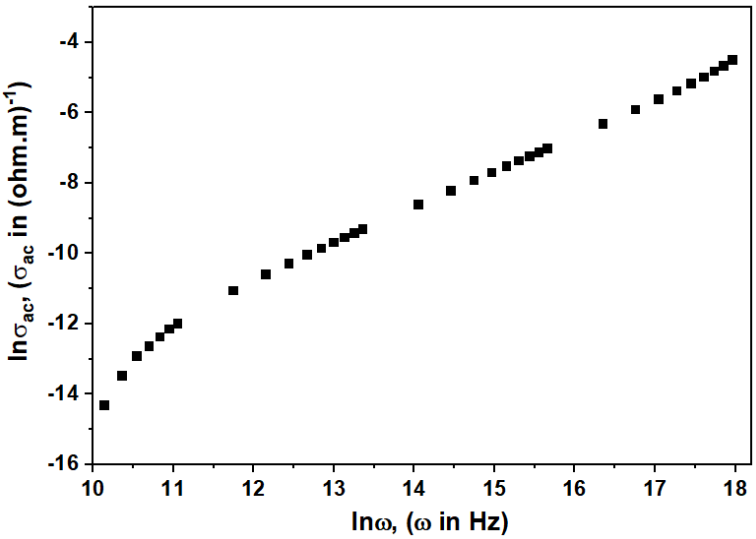

Figure 10. The frequency dependence of the AC electrical conductivity for DFPDAEHPQD.

3.9. Antitumor activity of DFPDAEHPQD

Synthesized DFPDAEHPQD compound has been examined for its antitumor activity and cytotoxicity against two different human cancer cell lines HepG-2 and HCT-116. Results presented in Fig. 11 showed that DFPDAEHPQD exhibited strong antitumor activity against these two cell lines. This figure reflected that DFPDAEHPQD showed significant inhibition towards the proliferation of both used cell lines HepG-2 and HCT-116 in a dose-dependent manner. The treatment with DFPDAEHPQD decreased the proliferation of HepG-2 cells with a 50 % reduction at about 3.07 µg/ml. In comparison, HCT-116 cells showed a significant decrease in proliferation with a 50 % reduction at about 7.15 µg/ml of DFPDAEHPQD extract. The effect of DFPDAEHPQD concentration on the morphological features of both HepG-2 and HCT-116 cells is shown in Figs. (12&13). The Structure-activity relationship (SAR), in the present study, has focused on the influence of fluorine groups on the antitumor activity of the DFPDAEHPQD compound. Some recent studies depicted that compounds containing fluorine atoms (an electron-withdrawing group) strengthen the inhibitory activity of cancer cells [40,71,72]. This may be due to the high electronegativity of fluorine atoms (4.0 on Pauling's electronegativity scale) which causes increasing the lipophilicity of the molecule that enhances the absorption rate, and helps easy penetration of the compound through the lipid membranes and therefore boosts the intercellular drug delivery [40,73,74].

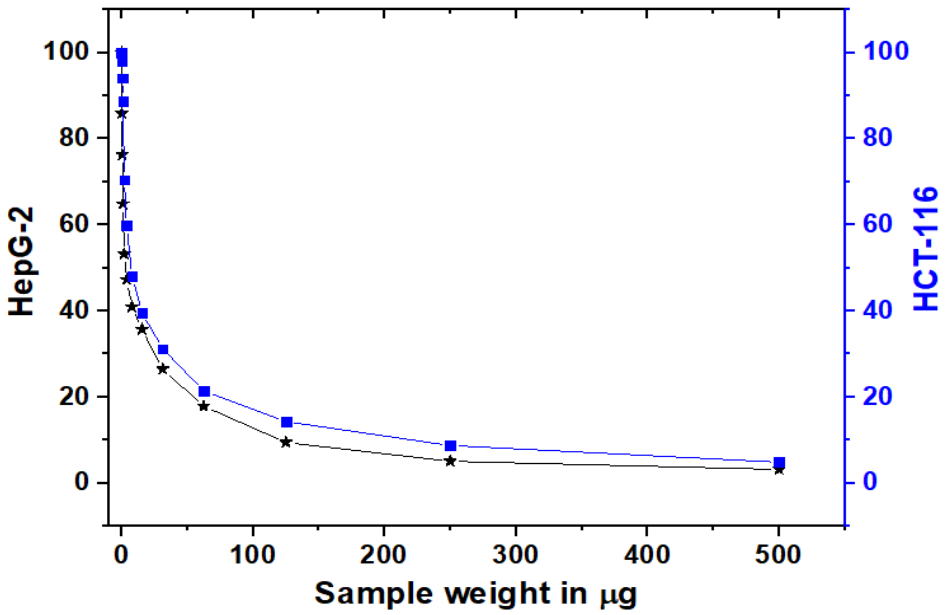

Figure 11. Effect of DFPDAEHPQD on the proliferation of HepG-2 and HCT-116 cells. Cells were treated with different concentrations of DFPDAEHPQD, incubated at 37°C, and harvested after 24 h.

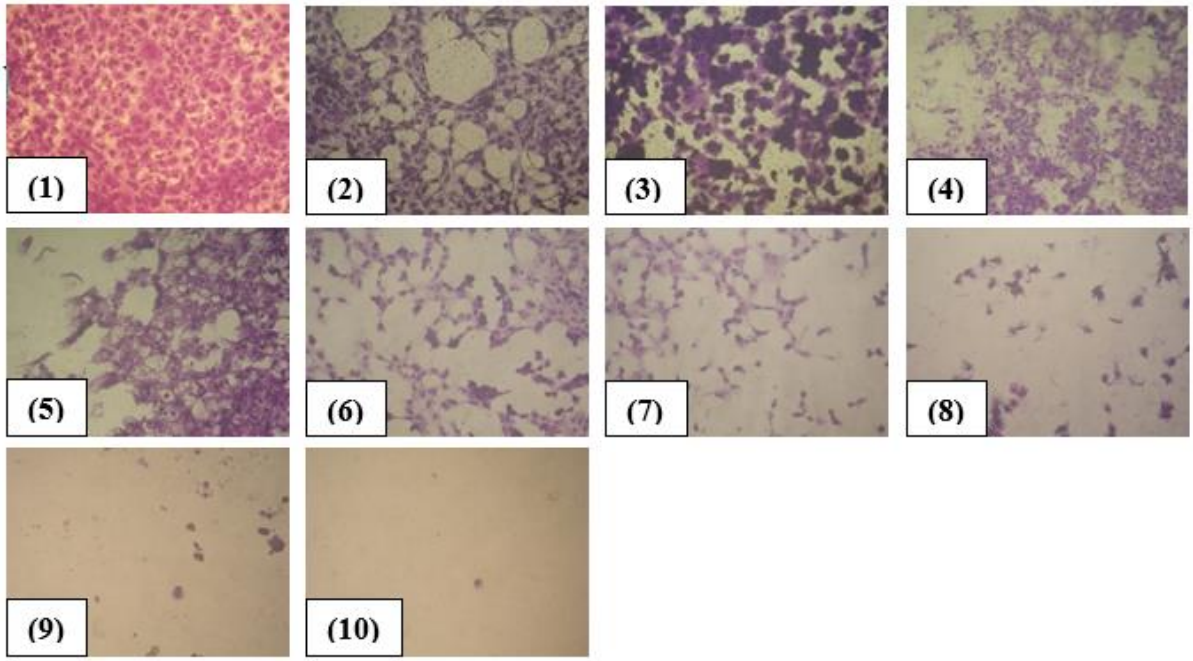

Figure 12. (1) HepG-2 cells (control), (2-10) HepG-2 cells treated with different concentrations of DFPDAEHPQD: (2) 2 µg/ ml; (3) 3.9 µg/ ml; (4) 7.8 µg/ ml; (5) 15.6 µg/ ml; (6) 31.25 µg/ ml; (7) 62.5 µg/ ml; (8) 125 µg/ ml; (9) 250 µg/ ml; (10) 500 µg/ ml.

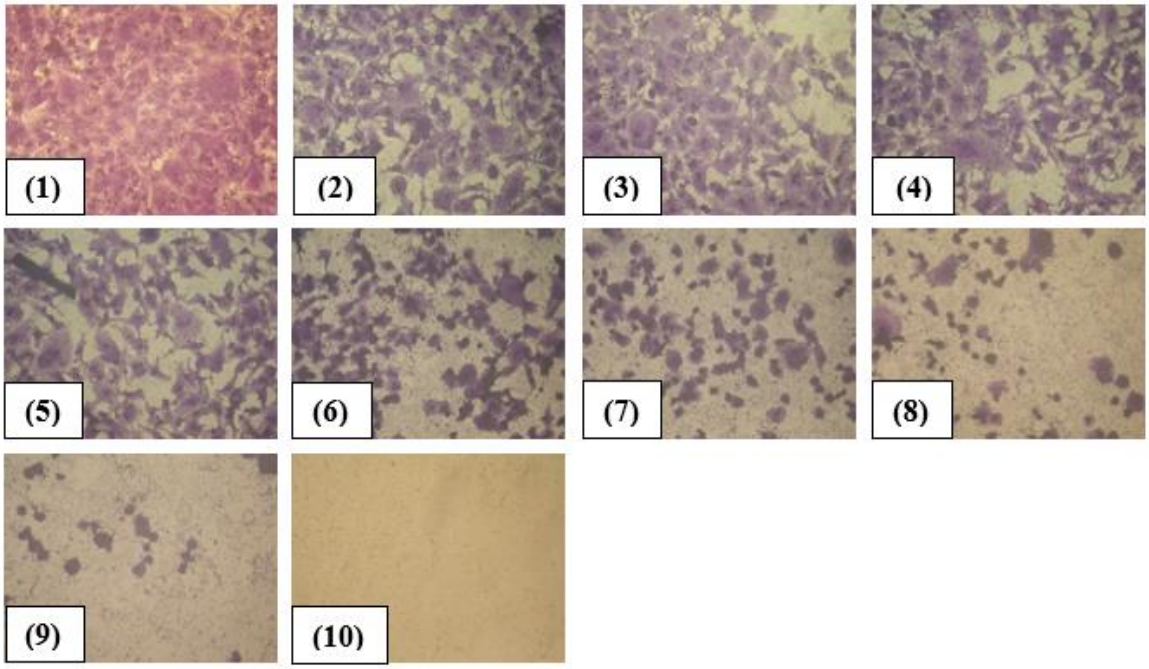

Figure 13. (1) HCT-116 cells (control), (2-10) HCT-116 cells treated with different concentrations of DFPDAEHPQD: (2) 2 µg/ ml; (3) 3.9 µg/ ml; (4) 7.8 µg/ ml; (5) 15.6 µg/ ml; (6) 31.25 µg/ ml; (7) 62.5 µg/ ml; (8) 125 µg/ ml; (9) 250 µg/ ml; (10) 500 µg/ ml.

Conclusion:

In conclusion, DFPDAEHPQD was successfully synthesized and characterized by various elemental analyses, FTIR, TGA, and XRD techniques. Fourier transform infrared spectroscopy analyzed the fingerprint function groups in DFPDAEHPQD. TGA was used to investigate the thermal characteristics of DFPDAEHPQD. Thermal analysis of DFPDAEHPQD indicated thermal stability over a large scale of temperature up to 300 ^{o}C. XRD analysis showed that the crystal of the used material is monoclinic with space group P_2. Optical diffused reflectance (ODR) of DFPDAEHPQD was utilized to measure bandgap energy and absorption region within the wavelength 190 – 2300 nm. The band optical gaps have been computed using Kubelka–Munk theory and found to be 2.35 and 2.25 eV for the direct and indirect transitions, respectively. DFPDAEHPQD is an organic semiconductor substance that is confirmed by the measurements of electrical conductivity of direct current. Results showed that the AC electrical conductivity of DFPDAEHPQD increases by raising the applied frequency. The dielectric constants were found to decrease with the increase in frequency, then they increase at higher values of photon frequency and get maximum value when the frequency reaches about 6×10^7 Hz. The dielectric loss was found to be lower than the dielectric constants. Moreover, DFPDAEHPQD showed promising antitumor activity and cytotoxicity against two human cancer cell lines (HepG-2 and HCT-116) with the corresponding IC_{50} values of 3.07 and 7.15 μg/ml, respectively. Thus, DFPDAEHPQD looks like organic material very efficiently; it is expected to have many safe applications in modern technology.

Acknowledgment

The authors would like to acknowledge the King Khalid University, Saudi Arabia for fruitful collaborations and technical support of this research. Furthermore, the authors are grateful to Prof. Dr. Hany M. Hassanin, Department of Chemistry, Faculty of Education, Ain Shams University, for synthesizing this research material.

References:

1. I. El Ouedghiri-Idrissi, M. Lougdali, Z. Makir, O.A. Niasse, Z. Sofiani, Photoluminescence of organic thin film Copper phthalocyanine CuPc for LED application. Materialstoday: PROCEEDINGS, **66**(1) (2022) 76-79. https://doi.org/10.1016/j.matpr.2022.03.294
2. O. Bolton, K. Lee, H.J. Kim, K.Y. Lin, J. Kim, Activating efficient phosphorescence from purely organic materials by crystal design. Nature Chemistry, **3** (2011) 205-210. https://doi.org/10.1038/nchem.984
3. J. Chen and Y. Cao, Development of novel conjugated donor polymers for high-efficiency bulk-heterojunction photovoltaic devices. Acc. Chem. Res., **42** (2009) 1709-1718 https://doi.org/10.1021/ar900061z

4. S. Heeb; M.P. Fletcher; S.R. Chhabra; S.P. Diggle; P. Williams; M. Cámara, "Quinolones: from antibiotics to autoinducers". FEMS Microbiology Reviews, **35**(2) (2011) 247–274. https://doi.org/10.1111/j.1574-6976.2010.00247.x
5. C.C. Wu, T.K. Li, L. Farh, L.Y. Lin, T.S. Lin, Y.J. Yu. Structural basis of type II topoisomerase inhibition by the anticancer drug etoposide. Science, **333** (2011) 459-462. https://doi.org/10.1126/science.1204117
6. A.K. McClendon, N. Osheroff. DNA topoisomerase II, genotoxicity, and cancer. Mutat Res, **623** (2007) 83-97. https://doi.org/10.1016/j.mrfmmm.2007.06.009
7. L.S. Cavalcante, J.C. Sczancoski, M.S. Li, E. Longo and J.A. Varela, β-$ZnMoO_4$ microcrystals synthesized by the surfactant-assisted hydrothermal method: Growth process and photoluminescence properties. Colloids and Surfaces A: Physicochem. Eng. Aspects, **396** (2012) 346-351. http://dx.doi.org/10.1016/j.colsurfa.2011.12.021
8. T. Li, S. Zhao, X. Sheng, L. Ji, Y. Jiang, F. Wang, J. Liu, and Ch. Luo, Enhanced protection of manganese-doped zinc molybdate with synergistic corrosion resistance effects. Progress in Organic Coatings, **182** (2023) 107617 https://doi.org/10.1016/j.porgcoat.2023.107617
9. X. Sheng, L. Zhou, X. Guo, X. Bai, X. Liu, J. Liu, and Ch. Luo, Composition design and anticorrosion performance optimization of zinc molybdate pigments. Materials Today Communications, **28** (2021)102477 https://doi.org/10.1016/j.mtcomm.2021.102477
10. N.A. El-Ghamaz, A.Z. El-Sonbati, M.A. Diab, A.A. El-Bindary, M.K. Awad and Sh.M. Morgan, Dielectrical, conduction mechanism and thermal properties of rhodanine azodyes. Mater. Sci. Semicond. Process, **19** (2014) 150-162. http://dx.doi.org/10.1016/j.mssp.2013.12.005
11. H. Abdeldjebar, Ch. A. Terbouche, A. Terbouche, and H. Lakhdari, Exploring Schiff base ligand inhibitor for cancer and neurological cells, viruses and bacteria receptors by homology modeling and molecular docking. Computational Toxicology, **23** (2022) 100231 https://doi.org/10.1016/j.comtox.2022.100231
12. M. N. Matada and K. Jathi, A novel azo metal complexes of 5, 5, 7-trimethyl-4, 5, 6, 7-tetrahydro-1, 3-benzothiazole as potential pharmacological agents: Synthesis and spectroscopic characterization. Journal of Molecular Structure, **1180** (2019) 196-208 https://doi.org/10.1016/j.molstruc.2018.11.081
13. J.W. Moore; C.L. Stanitski, P.C. Jurs, Principles of Chemistry: The Molecular Science. Belmont: (2010). Brooks/Cole. https://en.wikipedia.org/wiki/Special:BookSources/978-0-495-39079-4
14. D. O'Hagan. "Understanding Organofluorine Chemistry. An Introduction to the C–F Bond". Chemical Society Reviews, **37**(2) (2008) 308–319. https://doi.org/10.1039/B711844A
15. Riedel, Sebastian; Kaupp, Martin. "The highest oxidation states of the transition metal elements". Coordination Chemistry Reviews, **253**(5–6) (2009) 606-624. https://doi.org/10.1016/j.ccr.2008.07.014
16. L.R. Arana; N. Mas; R. Schmidt; A.J. Franz; M.A. Schmidt; K.F. Jensen, "Isotropic Etching of Silicon in Fluorine Gas for MEMS Micromachining". Journal of Micromechanics and Microengineering, **17**(2) (2007) 384. DOI 10.1088/0960-1317/17/2/026
17. A.T. Proudfoot; S.M. Bradberry; J.A. Vale, "Sodium Fluoroacetate Poisoning". Toxicological Reviews, **25**(4): (2006) 213–219. https://doi.org/10.2165/00139709-200625040-00002
18. C.A. Yeung, "A Systematic Review of the Efficacy and Safety of Fluoridation". Evidence-Based Dentistry, **9**(2) (2008) 39–43. https://doi.org/10.1038/sj.ebd.6400578

19. L.A. Johnson,). "Against Odds, Lipitor Became World's Top Seller". (28 December (2011) The Boston Globe. Retrieved 24 October (2013).

20. W.K. Hagmann "The Many Roles for Fluorine in Medicinal Chemistry". Journal of Medicinal Chemistry, **51**(15) (2008) 4359–4369.
https://doi.org/10.1021/jm800219f

21. FDA Drug Safety Communication: FDA advises restricting fluoroquinolone antibiotic use for certain uncomplicated infections; warns about disabling side effects that can occur. FDA (2016)

22. T. Lewis and J. Cook, Fluoroquinolones and Tendinopathy: A Guide for Athletes and Sports Clinicians and a Systematic Review of the Literature, Journal of Athletic Training, **49**(3) (2014) 422–427
https://doi.org/10.4085/1062-6050-49.2.09

23. Sh.A. Tandon, R. Kumar, R.K. Bajwa, S.A. Yadav, Pytoremediation of fluoroquinolone group of antibiotics from wastewater. Natural Science, **5**(12A) (2013) 21-27.
http://www.scirp.org/journal/PaperInformation.aspx?PaperID=41500

24. J. Boogaard, G.S. Kibiki, E.R. Kisanga, M.J. Boeree, R.E. Aarnoutse. New drugs against tuberculosis; problems, progress, and evaluation of agents in clinical development. Antimicrob Ag Chemother, **53** (2009) 849-862.
https://doi.org/10.1128/aac.00749-08

25. T.S. Murray, R.S. Baltimore. Pediatric uses of fluoroquinolone antibiotics. Pediatr Ann, **36** (2007) 336-342.
https://doi.org/10.3928/0090-4481-20070601-09

26. L. Sung, A. Manji, J. Beyene, et al. "Fluoroquinolones in children with fever and neutropenia: a systematic review of prospective trials". The Pediatric Infectious Disease Journal, **31**(5) (2012) 431–5.
https://doi.org/10.1097/INF.0b013e318245ab48

27. J.S. Bradley, A. Arguedas, J.L. Blumer, X. Saez-Llorens, R. Melkote, G.J. Noel. Comparative study of levofloxacin in the treatment of children with communityacquired pneumonia. Pediatr Infect Dis J, **26** (2007) 868-878.
https://doi.org/10.1097/inf.0b013e3180cbd2c7

28. S.A. Al-Trawneh, J.A. Zahra, M.R. Kamal, M.M. El-Abadelah, F. Zani, M. Incerti. Synthesis and biological evaluation of tetracyclic fluoroquinolones as antibacterial and anticancer agents. Bioorg Med Chem, **18** (2010) 5873-5884.
https://doi.org/10.1016/j.bmc.2010.06.098

29. D. Jia, X. You, M. Tang, Y, Lyu, J. Hu, and W. Sun, Single and combined genotoxicity of metals and fluoroquinolones to zebrafish embryos at environmentally relevant concentrations. Aquatic Toxicology, **258** (2023) 106495
https://doi.org/10.1016/j.aquatox.2023.106495

30. P. Bhattacharya, S. Mukherjee, and S.M. Mandal, Fluoroquinolone antibiotics show genotoxic effect through DNA-binding and oxidative damage. Spectrochim. Acta, Part A, **227** (2020) 117634.
https://doi.org/10.1016/j.saa.2019.117634

31. H. K. Swedan, A. E. Kassab, E. M. Gedawy, and S. E. Elmeligie, Topoisomerase II inhibitors design: Early studies and new perspectives. Bioorganic Chemistry, **136** (2023) 106548.
https://doi.org/10.1016/j.bioorg.2023.106548

32. K.E. Hevener, T.A. Verstak, K.E. Lutat, D. L. Riggsbee, and J.W. Mooney, Recent developments in topoisomerase-targeted cancer chemotherapy. Acta Pharmaceutica Sinica B, **8**(6) (2018) 844-861.
https://doi.org/10.1016/j.apsb.2018.07.008

33. R. Nagavath, S.K. Nukala, N. Sirassu, R.R. Sagam, R. Manchal, S. Paidakula, and N.S. Thirukovela, One-pot synthesis of some new regioselective 4β-pyrazolepodophyllotoxins as DNA topoisomerase-II targeting anticancer agents. Journal of Molecular Structure, **1250**(2) (2022) 131724.
https://doi.org/10.1016/j.molstruc.2021.131724

34. W.P. Walters; J. Green; J.R. Weiss; M.A.J. Murcko, What do medicinal chemists actually make? A 50-year retrospective. Med. Chem, **54** (2011) 6405-6416 and references therein.
https://doi.org/10.1021/jm200504p

35. M.D. Aytemir; U. Calıs, Synthesis of some novel mannich bases derived from allomaltol and evaluation of their anticonvulsant activities. Hacettepe University Journal of the Faculty of Pharmacy, **27** (2007) 1-10. https://dergipark.org.tr/en/pub/hujpharm/issue/49849/639182

36. N.M. Aljamali, Review in azo compounds and its biological activity. Biochem Anal Biochem, **4**:2 (2015) 1-4. http://dx.doi.org/10.4172/2161-1009.1000169

37. E. Węglarz-Tomczak and Ł. Górecki, Azo dyes – biological activity and synthetic strategy. CHEMIK, **66**(12) (2012) 1298-1307.

38. C.N.D. Attoh, J. Adu, C.A. Danquah, Y. Jibira, P. Gyan, E.B.A. Adusei and C.D. Amengor, Antimicrobial, Antioxidant, and Anti-inflammatory Evaluation of Synthesised Azo Compounds based on β-naphthol, Catechol and Quinol Nucleus. Journal of Pharmaceutical Research International, **34**(42B) (2022) 48-64. http://dx.doi.org/10.9734/jpri/2022/v34i42B36304

39. T. Kappe; R. Aigner; P. Hohengassner, W. Stadlbauer, Syntheses of 3-Acyl-4-hydroxy-2(1H)quinolones. J. Prakt. Chem, **336** (1994) 596-601.

40. A.M. Saeed, S.S. AlNeyadi, and I.M. Abdou, Anticancer activity of novel Schiff bases and azo dyes derived from 3-amino-4-hydroxy-2H-pyrano [3, 2-c] quinoline-2, 5 (6H)-dione. Heterocyclic Communications, **26**(1) (2020) 192-205. https://doi.org/10.1515/hc-2020-0116

41. H.M. Hassanin, R.A. Serya, W.R. Abd Elmoneam, and M.A. Mostafa, Synthesis and molecular docking studies of some novel Schiff bases incorporating 6-butylquinolinedione moiety as potential topoisomerase IIβ inhibitors. Royal Society open science, **5**(6) (2018) 172407. https://doi.org/10.1098/rsos.172407

42. I.S. Yahia, H.Y. Zahran, F.H. Alamri, Pyronin Y as new organic semiconductors: Structure, optical spectroscopy, and electrical/dielectric properties. Synthetic Metals, **218** (2016) 19–26. https://doi.org/10.1016/j.synthmet.2016.04.024

43. H.M. Hassanin, W.R. Abd Elmoneam, M.A. Mostafa, Synthesis and antitumor activity evaluation of different 2,5-dialkyloxazolopyrano[3,2-c] quinolinone derivatives. Medicinal Chemistry Research, **28** (2019) 28–38. https://doi.org/10.1007/S00044-018-2259-9

44. S.M. Gomha, S.M. Riyadh, E.A. Mahmmoud, M.M. Elaasser, Synthesis and anticancer activities of thiazoles, 1,3-thiazines, and thiazolidine using chitosan-grafted-poly(vinyl pyridine) as a basic catalyst. Heterocycles, **91**(6) (2015) 1227–1243. https://doi.org/10.3987/COM-15-13210

45. X.Wang, W. Wang, Y. Liu, M. Ren, H. Xiao, and X. Liu, Characterization of conformation and locations of C–F bonds in graphene derivative by polarized ATR-FTIR. Analytical chemistry, **88**(7) (2016) 3926-3934. https://doi.org/10.1021/acs.analchem.6b00115

46. M. Hajfathalian, K.D. Gilroy, A. Yaghoubzade, A. Sundar, T. Tan, R.A. Hughes, S. Neretina, Photocatalytic enhancements to the reduction of 4-nitrophenol by resonantly excited triangular gold–copper nanostructures. J. Phys. Chem. C, **119** (2015) 17308−17315. http://dx.doi.org/10.1021/acs.jpcc.5b04618

47. K.D. Gilroy, R.A. Hughes, S. Neretina, Kinetically controlled nucleation of silver on surfactant-free gold seeds. Journal of the American Chemical Society, **136**(43) (2014) 15337-15345. https://doi.org/10.1021/ja5081635

48. Z.L.S. Seow, A.S.W. Wong, V. Thavasi, R. Jose, S. Ramakrishna and G.W. Ho, Controlled synthesis and application of ZnO nanoparticles, nanorods, and nanospheres in dye-sensitized solar cells. Nanotechnology, **20** (2009) 045604 (6pp) https://doi.org/10.1088/0957-4484/20/4/045604

49. L. Tong, Q. Wei, A. Wei, and J.X. Cheng, Gold nanorods as contrast agents for biological imaging: optical properties, surface conjugation, and photothermal effects. Photochemistry and Photobiology, **85**(1) (2009) 21-32. https://doi.org/10.1111/j.1751-1097.2008.00507.x

50. X. Huang, S. Neretina, M.A. El-Sayed, Gold nanorods: from synthesis and properties to biological and biomedical applications. Advanced Materials, **21**(48) (2009) 4880-4910.
https://doi.org/10.1002/adma.200802789

51. A.A.M. Farag and I.S. Yahia. Rectification and barrier height are inhomogeneous in Rhodamine B-based organic Schottky diode. Synth Metals, **161** (2011) 32-39.
https://doi.org/10.1016/j.synthmet.2010.10.030

52. K. SowriBabun, A. Ramachandra Reddy, Ch. Sujatha, K. Venugopal Reddy, Effects of precursor, temperature, surface area, and excitation wavelength on photoluminescence of ZnO/mesoporous silica nanocomposite. Ceramics International, **39** (2013) 3055-3064.
http://dx.doi.org/10.1016/j.ceramint.2012.09.085

53. W.C. Zhang, X.L. Wu, H.T. Chen, J. Zhu, G.S. Huang, Excitation wavelength dependence of the visible photoluminescence from amorphous ZnO granular films. J. Appl. Phys, **103** (2008) 093718.
https://doi.org/10.1063/1.2924421

54. F. El-Kabbany, S. Taha, M. Hafez, A study of the phase transition of reheated diphenyl carbazide (DPC) by using UV spectroscopy. Spectrochimica Acta Part A: Molecular and Biomolecular Spectroscopy, **128** (2014) 481–488.
https://doi.org/10.1016/j.saa.2014.02.143

55. W. Brütting, ed., Physics of Organic Semiconductors, 2nd, Completely New Revised Edition, WILEY-VCH Verlag, (2012).
ISBN: 978-3-527-41053-8

56. J. Tauc, R. Grigorovici, and A. Vancu, Optical properties and electronic structure of amorphous germanium. Phys. Status Solidi, **15** (1966) 627–637.
https://doi.org/10.1002/pssb.19660150224

57. C. Aydın, M.S. Abd El-Sadek, Kaibo Zheng, I.S. Yahia, F. Yakuphanoglu, Synthesis, diffused reflectance and electrical properties of nanocrystalline Fe-doped ZnO via sol–gel calcination technique. Optics & Laser Technology, **48** (2013) 447–452.
http://dx.doi.org/10.1016/j.optlastec.2012.11.004

58. M.S. El-Bana, M.S. Alkhalifah, and I.M. El Radaf, Novel and promising material (CuInSn3S8) for photovoltaic and optoelectronic applications. Surfaces and Interfaces, **31** (2022) 102037.
https://doi.org/10.1016/j.surfin.2022.102037

59. E.A. Davis, N.F. Mott, Conduction in non-crystalline systems V. Conductivity, optical absorption and photoconductivity in amorphous semiconductors. Philos. Mag, **22**(179) (1970) 903-922. Published online: 20 Aug (2006).
https://doi.org/10.1080/14786437008221061

60. I.S. Yahia, H.Y. Zahran, F.H. Alamri, Pyronin Y as new organic semiconductors: Structure, optical spectroscopy, and electrical/dielectric properties. Synthetic Metals, **218** (2016) 19–26.
https://doi.org/10.1016/j.synthmet.2016.04.024

61. V. Kumar, M. Gohain, V. Kumar, J.H.V. Tonder, B.C.B. Bezuidenhoudt, O.M. Ntwaeaborwa, H.C. Swart, Synthesis of quinoline based heterocyclic compounds for blue lighting application. Optical Materials, **50** (2015) 275–281.
https://doi.org/10.1016/j.optmat.2015.11.009

62. Sh.A. Mansour, I.S. Yahia, F. Yakuphanoglu, The electrical conductivity and dielectric properties of C.I. Basic Violet 10, Dyes Pigm, **87**(2) (2010) 144–148.
https://doi.org/10.1016/j.dyepig.2010.03.011

63. A.K. Jonscher. The 'universal' dielectric response. Nature, **267** (1977) 673-679.
https://doi.org/10.1038/267673a0

64. S. Bhattacharyya, S.K. Saha, M. Chakravorty, B.M. Mandal, D. Chakravorty, K. Goswami., Frequency-dependent conductivity of interpenetrating polymer network composites of polypyrrole–poly(vinyl acetate). Journal of Polymer Science Part B: Polymer Physics, **39**(16) (2001) 1935-1941.
https://doi.org/10.1002/polb.1168

65. V.M. Jali, S. Aparna, Sanjeev Ganesh, S.B. Krupanidhi. AC conductivity studies on the electron irradiated $BaZrO_3$ ceramic. Nucl Instruments Methods Phys Res B, **257**(1-2) (2007) 505-509. https://doi.org/10.1016/j.nimb.2007.01.167

66. V. Bobnar, A.Levstik, C. Huang and Q.M. Zhang; Distinctive Contributions from organic filler and relaxorlike polymer matrix to the dielectric response of CuPc-P(VDF-TrFE-CFE) composite. Phys. Rev. Lett., **92** (2004) 047604. https://doi.org/10.1103/physrevlett.92.047604

67. S.I. Qashou, Dielectric relaxation properties, and AC conductivity of Erbium(III)-Tris(8-hydroxyquinolinato) nanostructured films. Physica B: Condensed Matter, **649** (2023) 414421. https://doi.org/10.1016/j.physb.2022.414421

68. G. Ju-ka and Pivrikas, Private Communications, (2008).

69. F. Yakuphanoglu, Y. Aydogdu, U. Schatzschneider, E. Rentschler, DC and AC conductivity and dielectric properties of the metal-radical compound: Aqua[bis(2-dimethylaminomethyl-4-NIT-phenolato)]copper(II). Solid State Communications, **128**(2-3) (2003) 63-67. https://doi.org/10.1016/S0038-1098(03)00651-3

70. N.A. Hegab, M.A. Afifi, H.E. Atyia and M.I. Ismael, Ac Conductivity and Dielectric Properties of Amorphous $Ge_{15}Se_{60}X_{25}$ (X = As or Sn) Films. Acta Physica Polonica A, **3** (2011) 416–423. https://doi.org/10.12693/APhysPolA.119.416

71. F.R. Leroux, B. Manteau, J.P. Vors, and S. Pazenok, Trifluoromethyl ethers–synthesis and properties of an unusual substituent. Beilstein journal of organic chemistry, **4**(1) (2008) 13. https://doi.org/10.3762/bjoc.4.13

72. E. Castagnetti and M. Schlosser, The Trifluoromethoxy Group: A Long-Range Electron-Withdrawing Substituent, Chemistry–A European Journal, **8**(4) (2002) 799-804. https://doi.org/10.1002/1521-3765(20020215)8:4<799::AID-CHEM799>3.0.CO;2-6

73. M.A. Mostafa, Synthesis, anticancer evaluation, and molecular docking study of novel 4-hydroxybenzo [*h*][1,6] naphthyridine-2, 5-dione derivatives. Journal of Physical Organic Chemistry, **36**(2) (2023) e4429. https://doi.org/10.1002/poc.4429

74. M. Žukauskas, B. Grybaitė, P. Jonutė, R. Vaickelionienė, P. Gibieža, G. Vaickelionis, B. Dragūnaitė, K. Anusevičius, V. Mickevičius, V. Petrikaitė, Evaluation of N-aryl-β-alanine derivatives as anticancer agents in triple-negative breast cancer and glioblastoma in vitro models. Bioorg. Chem, **115** (2021) 105214. https://doi.org/10.1016/j.bioorg.2021.105214